Study on Electrochemical Performance of Alloy Inert Anodes in Low-Temperature Aluminium Electrolytes

Dan Liu[1], Dongsheng Li[2], Yanan Zhang[3], Shengzhong Bao[4] and Guisheng Liang[5]
1, 2, 5. Intermediate Engineer
3, 4. Senior Engineer
Zhengzhou Non-ferrous Metals Research Institute of Chalco (ZRI), Zhengzhou, China
Corresponding author: dan_liu690@chinalco.com.cn
https://doi.org/10.71659/icsoba2025-al071

Abstract

During electrolysis in low temperature aluminium electrolyte systems at 1073 K, with bath ratios of 1.15, 1.25 and 1.35, respectively, the anode potential and self-corrosion potentials of the alloy inert anode tend to decrease with increasing bath ratios. The decomposition voltage of alumina increases with increasing bath ratios. When electrolysis is carried out in low-temperature electrolytes with higher bath ratio (1.35), the degree of electrochemical reaction on the surface of the alloy anode is stronger, and the self-corrosion potential of the alloy anode is smaller (0.25 V), with a larger trend of self-corrosion. Pre-melting the low-temperature aluminium electrolyte before electrolysis not only enhances the uniformity of electrolyte composition but also inhibits the hydrolysis reaction between AlF_3 and adsorbed water, thereby suppressing HF gas generation. This reduces anode corrosion, extends anode service life, and stabilizes long-term electrolysis processes.

Keywords: Alloy inert anodes, Low temperature aluminium electrolysis, Electrochemical properties, Bath ratio, Anode potential.

1. Introduction

The traditional aluminium industry uses carbon as anode material, and there are many problems: (1) large consumption of materials, requiring a huge processing anode plant, with high investment and production costs; (2) carbon anodes need to be replaced, causing high labour intensity; (3) due to the continuous consumption of the carbon anodes, the interpolar distance is unstable; (4) the electrolysis reaction produces a large amount of greenhouse gases, including PFC (perfluorocarbon) gases and asphalt fumes emission, which causes pollution of the environment. Alternatively, the use of inert anodes in the process of aluminium electrolysis has the following advantages: (1) electrodes are not consumed, which reduces the production cost; (2) the interpolar distance is stable and easy to control; (3) the anode is replaced less often, which reduces the intensity of labour; (4) a higher anode current density can be used, which increases the capacity of electrolysis cells; (5) the anode product is oxygen, which avoids environmental pollution [1, 2].

The theoretical decomposition voltage for aluminum electrolysis of alumina with inert anodes is about 1 V higher than that of carbon anodes. But for an inert anode with a wettable cathode, the interpolar distance can be reduced, maybe down to 1 cm. In addition, the inert anode oxygen precipitation overpotential is lower than the carbon anode overpotential. Thus, it may be possible that the inert anode cell technology can give energy consumptions close to the values for the best traditional cells.

Inert anodes is now the focus of attention and research of the international aluminium industry and materials community. The research on inert anodes mainly focuses on the selection of anode materials. Since metal anodes possess better electrical and thermal conductivity and mechanical processing properties than ceramic anodes and cermet anodes, they have been the focus of

attention of the aluminium industry and the materials science community. The inert anodes are considered to be one of the most promising anode materials for aluminium electrolysis [3–12]. In this paper, the electrochemical performance of a copper-iron aluminium-based alloy inert anode in low temperature aluminium electrolyte at 1073 K (≈ 800 °C) is investigated to provide technical support for the use of alloy inert anodes in a low temperature aluminium electrolyte.

2. Experimental

Before the test, the working electrode and reference electrode need to be prepared. The inert anode of copper-iron-aluminium base alloy to be tested was machined into a working electrode in the shape of a cylinder, which was connected to the guide rod of a copper rod and then covered with a corundum protective tube to expose its working area. A certain mass of crushed 5N (99.999 %) high-purity aluminium was loaded into a corundum blind tube with a diameter of 1 mm hole 10 mm from the bottom. Then a tungsten wire guide rod with a diameter of 1 mm and a length of 100 mm longer than that of the blind tube was put into the corundum blind tube. Finally, the corundum blind tube was placed into a high-temperature pit-type furnace protected by argon, and then taken out after 10 min at 1023 K. The high-purity aluminium reference electrode was prepared. The prepared working electrode and reference electrode were fixed together on a BN base.

A certain mass of electrolyte of the NaF-KF-AlF_3-6 wt.% Al_2O_3 system (Bath ratio CR = ([NaF] + [KF]) / [AlF_3]) was weighed and loaded into a high-purity graphite crucible and vibrated. Then the working electrode and reference electrode fixed on the BN base were placed on top of the electrolyte, and the graphite crucible was covered. The graphite crucible was placed in the high-temperature pit-type furnace, then covered with the furnace lid, the protective gas conduit was connected, and the thermocouple put in. Finally, the argon protective gas was turned on, and the heating started according to the procedure up to the test temperature, this last being maintained constant for a certain period of time.

Before the start of the electrochemical test, the three-electrode system was connected: working electrode, reference electrode and counter electrode (the counter electrode for this test was a high-purity graphite crucible, and the guide rod was a stainless-steel rod connected to it). The electrochemical workstation used for the test was an IM6 electrochemical workstation from Zahner, Germany. The schematic diagram of the test setup and the three electrodes are shown in Figures 1 and 2.

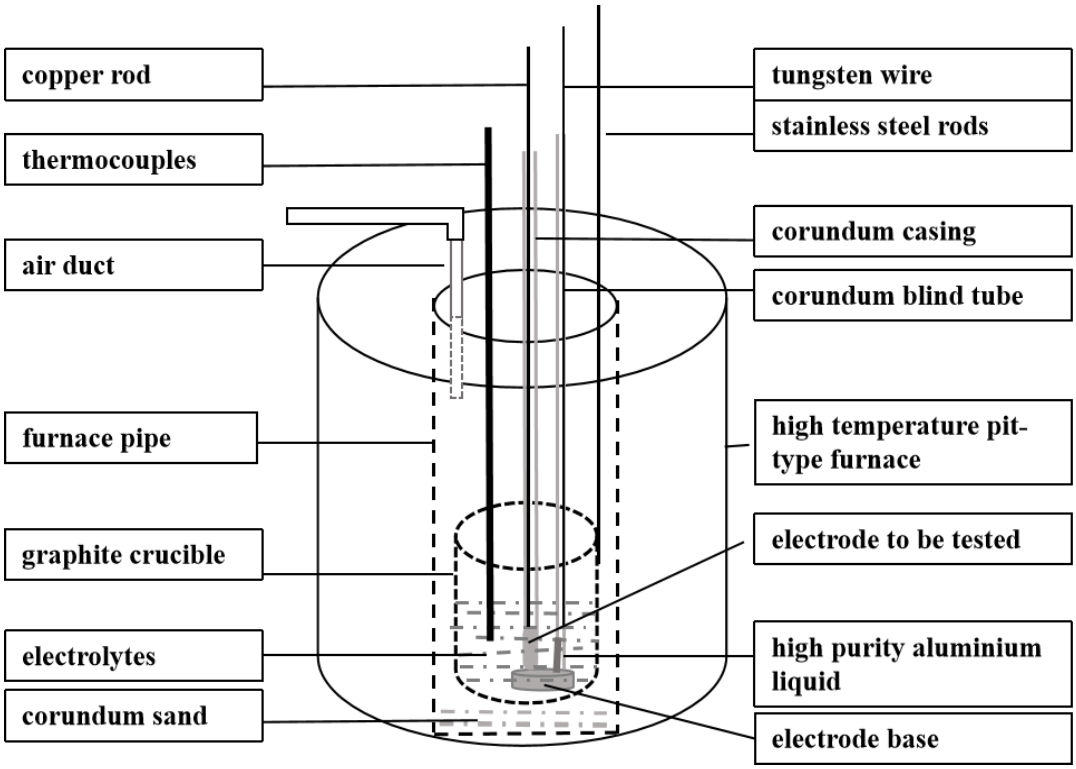

Figure 1. Schematic diagram of the test setup.

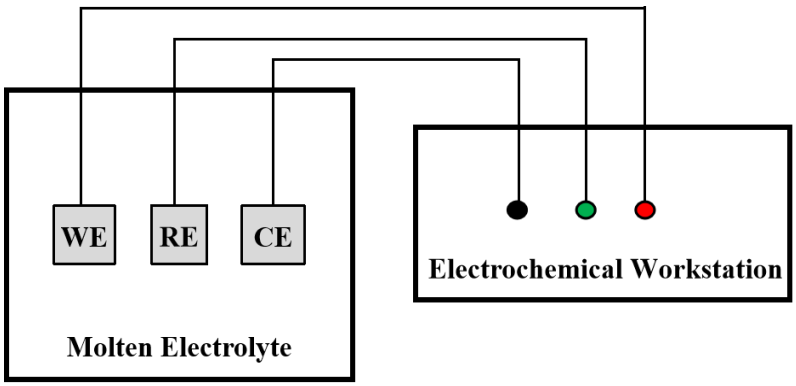

Figure 2. Schematic diagram of three-electrode connection.
WE- Work Electrode; RE- Reference Electrode; CE- Counter Electrode.

3. Results and Discussion

3.1 Linear Scanning Voltammetric Curve

Before electrolysis at 1073 K with constant current (i = 5 A/cm^2), the linear scanning voltammetry curves (E-i curves) of the alloy anode in low-temperature aluminium electrolytes with bath ratios of 1.15, 1.25, and 1.35, respectively, are shown in Figure 3. The shapes and numbers of current peaks in the four curves a, b, c and d after 1.0 V are more or less the same, and the location of the peaks is shifted to higher potentials with the increase of bath ratio, and the value of current density at the peaks is also increased with the increase of bath ratio. This is presumed to be due to the improvement of the conductivity of the aluminium electrolyte. An increase in bath ratio increases the concentration or activity of the conducting ions in the aluminium electrolyte and the ions move more readily, which also shows up as an increase in current on the E-i curve. This happens to also

explain that the electrochemical reaction of the alloy inert anode is a bit more intense in the low-temperature aluminium electrolyte with a high bath ratio (from curves a and c, it can be seen that the alloy inert anode has the smallest overall current density in the low-temperature aluminium electrolyte with a low molecular of 1.15, and the largest overall current density with a high bath ratio of 1.35). After the potential of 1 V, the appearance of the first three current peaks on the four curves may be attributed to the oxidation of Fe to produce FeO, the further oxidation of Fe to produce Fe_2O_3 and/or Fe_3O_4, and the oxidation of Fe and FeO at sufficient potential to produce Fe_2O_3 and or Fe_3O_4. The appearance of the last three current peaks may be attributed to the oxidation of Cu to produce Cu_2O, the oxidation of Cu_2O to produce CuO, and Cu fluorination reaction to produce CuF and or CuF_2.

As can be seen from the curves a, b, and c, the actual decomposition voltage of alumina in low-temperature aluminium electrolytes with different bath ratios at 1073 K does not differ much, which is about 2.34 V, 2.35 V, and 2.36 V in order, and the corresponding anodic overpotentials are 0.05 V, 0.06 V, and 0.07 V, respectively (the decomposition voltage of alumina at 1100 K is 2.29 V). Meanwhile, the self-corrosion potentials of the alloy anodes were different, which were decreasing with the increase of the bath ratio (a: 0.77 V, b: 0.69 V, and c: 0.25 V), which indicated that the alloy anodes had lower self-corrosion resistance and stronger tendency for a self-corrosion reaction to take place in low-temperature aluminium electrolytes with higher bath ratios.

As shown by curves c and d, the current density value of the alloy anode in the pre-melted low-temperature aluminium electrolyte before constant-current electrolysis is much lower than that in the non-pre-melted low-temperature aluminium electrolyte, and the alloy anode in the non-pre-melted low-temperature electrolyte has a high current peak at a voltage of about 0.5 V. This is probably due to the fact that the non-pre-melted low-temperature aluminium electrolyte generates HF gas during the heating process, which caused corrosion to the electrode, and the impurity peak caused by the electrochemical reaction that easily occurs after the energisation. Pre-melting shortens the duration of air exposure of the electrolyte, eliminates adsorbed water, and prevents the occurrence of hydrolysis reactions of aluminium fluoride due to the presence of adsorbed water, thereby reducing or inhibiting the production of HF gas. Therefore, considering the degree of electrochemical reaction of the alloy anode before electrolysis and energy saving, it may be more beneficial to protect the anode if the low-temperature aluminium electrolyte is pre-melted before the electrolysis test.

The linear scanning voltammetry curves of the alloy anodes in low-temperature aluminium electrolytes with bath ratios of 1.15, 1.25, and 1.35 after constant-current electrolysis ($i = 5$ A/cm^2) at 1073 K are shown in Figure 4. The shape and number of current peaks appearing in the four curves remain approximately the same. Compared with Figure 3, the overall current density values of curves a, b, and c are closer, and the self-corrosion potentials increase (a: 1.11 V, b: 1.12 V, and c: 1.02 V), which indicates that the substances on the anode surface of the alloy have been electrochemically reacted and the self-corrosion resistance has been reduced for all of them after constant current electrolysis. Curve c in Figure 4 has fewer impurity peaks than curve C in Figure 3, which indicates that a small amount of impurity elements in the aluminium electrolyte have been reacted away after constant current electrolysis. Comparing Figure 4 with Figure 3, all four curves have one less current peak located at 2.30 V. This may be due to the fact that the Cu elements participating in the reaction on the surface of the alloy anode participated in the electrochemical reaction during the electrolysis process and the reaction was complete after the constant current electrolysis. It can also be seen from Figure 4 that the decomposition voltage of alumina after constant-current electrolysis increased compared with that before constant-current electrolysis. It can be assumed that after constant-current electrolysis, the self-corrosion resistance of the alloy anode in the aluminium electrolyte decreases, and the surface material undergoes an electrochemical reaction in the electrolysis process to generate oxides. It can be hindered from further reacting with the electrolyte or oxygen due to the existence of the oxide film layer on the

surface, and therefore the current density change curve in the E-i curve after constant-current electrolysis (Figure 4) is relatively flat.

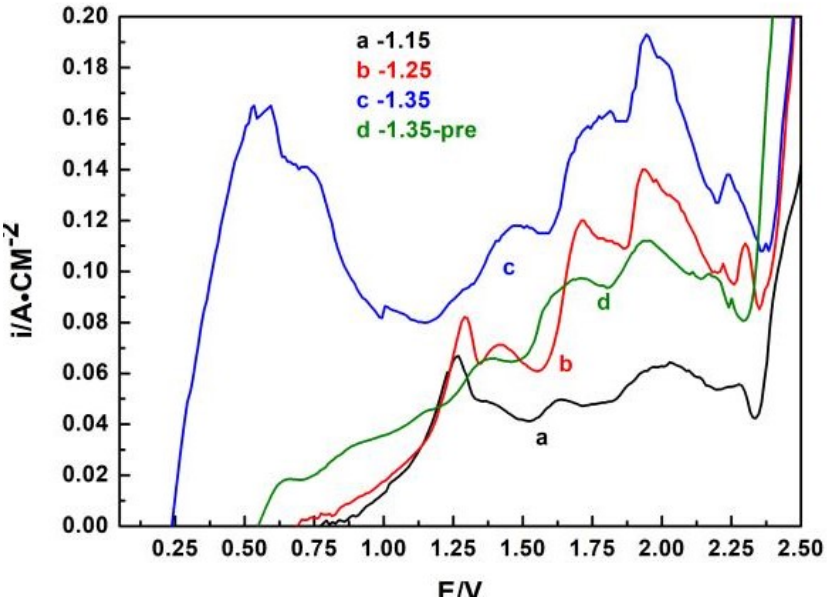

Figure 3. E-i curve of the alloy inert anode before constant current electrolysis, ν = 1 mV/s, T=1073 K

a. bath ratio of 1.15, unpremelted electrolyte before test
b. bath ratio of 1.25, unpremelted electrolyte before test
c. bath ratio of 1.35, unpremelted electrolyte before test
d. bath ratio of 1.35, pre-melted electrolyte before test.

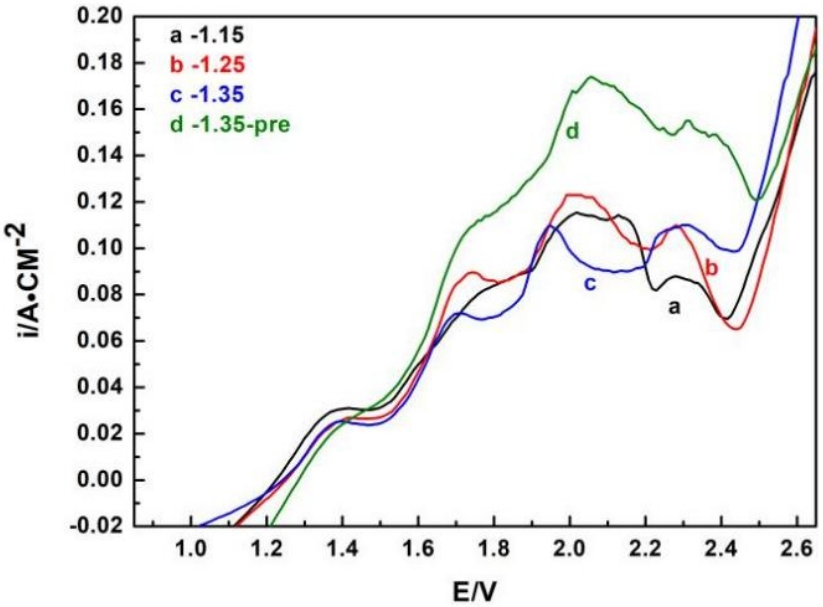

Figure 4. E-i curve of the alloy inert anode after constant current electrolysis, ν = 1 mV/s, T=1073 K：

a. bath ratio of 1.15, unpremelted electrolyte before test
b. bath ratio of 1.25, unpremelted electrolyte before test
c. bath ratio of 1.35, unpremelted electrolyte before test
d. bath ratio of 1.35, pre-melted electrolyte before test.

3.2 Constant Current Electrolysis Curve

The constant-current (set to 0.5 A/cm^2) electrolysis profiles of alloy anodes in low-temperature aluminium electrolytes with different bath ratios at 1073 K are shown in Figure 5. The constant temperature - constant current electrolysis interval is shown before 14 400 s, and the reduced temperature - constant current electrolysis interval is shown after 14 400 s.

From curves a, b and c in Figure 5, it can be seen that when the electrolyte was not pre-melted before the test, the overall potential of the constant-current electrolysis curve appeared to decrease and then increase with the increase of bath ratio. From curves c and d, it can be seen that the potential of constant-current electrolysis after the electrolyte is pre-melted is lower than that of constant-current electrolysis when the electrolyte is not pre-melted, which indicates that the step of pre-melting the electrolyte is advantageous to electrolysis. This is most likely due to the fact that the pre-melting electrolyte step prevents the hydrolysis of AlF_3 to produce HF gas, which reduces the degree of corrosion of the working electrode. Water is introduced via raw materials in the electrolyte system, existing in two forms: adsorbed water and bound water. The electrolyte system we used for the test was custom-formulated in our laboratory. Among them, the aluminium fluoride was prepared by us through a two-stage dehydration process, exhibiting significantly lower moisture content vs. conventional methods. From the test results, we think that the pre-melted electrolyte may eliminate or drastically reduce adsorbed water, inhibiting the hydrolysis of aluminium fluoride caused by it and reducing the production of HF gas. The electrolyte used in our experimental study has limited electrolyte volume and minimized adsorbed water content, the content of bound water is inherently negligible, and even if HF gas is produced during the electrolysis process, the corrosion of the electrodes is limited. Additionally, the pre-molten electrolyte exhibits uniform composition, minimizing the risk of compositional deviation. Therefore, it can be surmised that pre-melting may be able to protect the electrode and stabilized electrolysis. While laboratory results are promising, industrial reliability requires further validation through comprehensive scaling assessment.

It can be seen that at the beginning of the working potential there is an upward trend, which is largely due to the early stage of electrolysis, alumina decomposition to produce a gradual increase in the amount of oxygen. The oxygen collects on the surface of the working electrode, and it is easy to oxidise the Fe element of oxidation reaction occurs gradually to form the metal oxide film layer. The film layer in the electrolyte with the increase of time and potential shows a continuous trend of dissolution and formation. At the initial stage of constant-current electrolysis, a plateau appears on each curve, indicating that there is a stabilisation process of the metal oxide formed in this process. With the extension of time, the oxide film gradually thickens. When the potential gradually increases, the Cu element on the electrode surface and oxygen undergo oxidation reaction, and the metal oxide film layer gradually thickens. When the fluorination reaction of Cu elements on the electrolytic surface occurs, the voltage growth rate is accelerated. The d curve has the lowest electrolysis potential among the four curves, and the potential changes slowly, which is more suitable for electrolysis from the consideration of energy saving. The analysis results of the curves in Figure 5 are consistent with the results of the linear scanning voltammetry curves in Figure 3.

Comparing the *a*, *b*, *c* and *d* curves during the constant-current (0.5 A/cm^2) electrolysis at a temperature of 1073 K down to 963 K at a cooling rate of 278 K/min, the *a* curve electrolyte bath ratio of 1.15 in the experimental system was rapidly increased to 3.8 V at a temperature of 1050.8 K and two plateaus appeared on the potential curve. The potential was 3.58 V and the potential was sharp at a temperature of about 1063 K.

The cooling electrolysis curve of the *b* curve electrolyte system with bath ratio of 1.25 showed a relatively slow increase of the potential in the beginning of the 60 min period, and the anodic

voltage increased rapidly at a temperature of about 1031 K. In the cooling electrolysis process at constant current (0.5 A/cm^2), the potential increased rapidly in the first 45 min of temperature reduction. When the temperature is about 1031 K, the anodic voltage increased rapidly, and the potential increases to 4.0 V within 170 min of the temperature reduction, and the temperature is 991.6 K at this time. At approximately 12 000 seconds, the curve exhibits a sudden drop. This may be caused by the dissolution rate of the oxide film on the working electrode surface significantly exceeding its formation rate, leading to film delamination. Alternatively, it could result from abnormal fluctuations in the reference electrode at this moment. The next step is to conduct transparent cell electrolysis experiments to further determine the causes of these phenomena.

The *c* curve shows that in the electrolyte with bath ratio of 1.35, the anodic voltage increases rapidly when the voltage is higher than 3.26 V (and the temperature is lower than 1040.6 K), and the temperature of the electrolysis should be controlled at 1043 K or above. The *d* curve, on the other hand, clearly shows that the potential increase is slowly varying during the temperature reduction electrolysis and the overall potential decreases by about 0.25 V compared to the *c* curve. The potential increase starts to decrease at a temperature of 1013 K and a potential of about 2.99 V. The increase in the potential of the electrolyte is about 2.99 V when the temperature is reduced to 973 K. When the temperature was reduced to 973 K, the potential was 3.535 V. This may be due to the fact that as the temperature decreases, the mobility of the electrolyte decreases and the movement of the free ions decreases, resulting in an increase in resistance and an increase in potential.

The potential of curve *d* is significantly the lowest among the four curves. Compared to curve *c*, curve *d* exhibits a slower potential increase, which can be reasonably explained by the minimal hydrolysis reaction caused by adsorbed water of the pre-molten electrolyte during electrolysis. And the two-stage dehydration process yielding aluminum fluoride with low crystalline water content, combined with the limited quantity of electrolyte used in the experiment. This results in little to no generation of HF gas, thereby causing less corrosion to the working electrode. During electrolysis, the dissolution rate of the oxide film formed by oxidation on the working electrode surface is comparable to its formation rate, with the formation rate slightly exceeding the dissolution rate. Consequently, the electrode potential shows a gradual upward trend, maintaining relative stability over prolonged electrolysis.

The *c* and *d* curves show that after the electrolyte is pre-melted before the experiment, the alloy anode is less affected by the temperature during the electrolysis. And the corrosion resistance time is longer. It may be due to the fact that the bath ratio of the electrolyte increases after the pre-melting, and the working electrode in the relatively high bath ratio of the molten salt electrolyte and the oxygen combined with the oxide film will be denser, the thickness of the film will be moderate, and it is also relatively more stable.

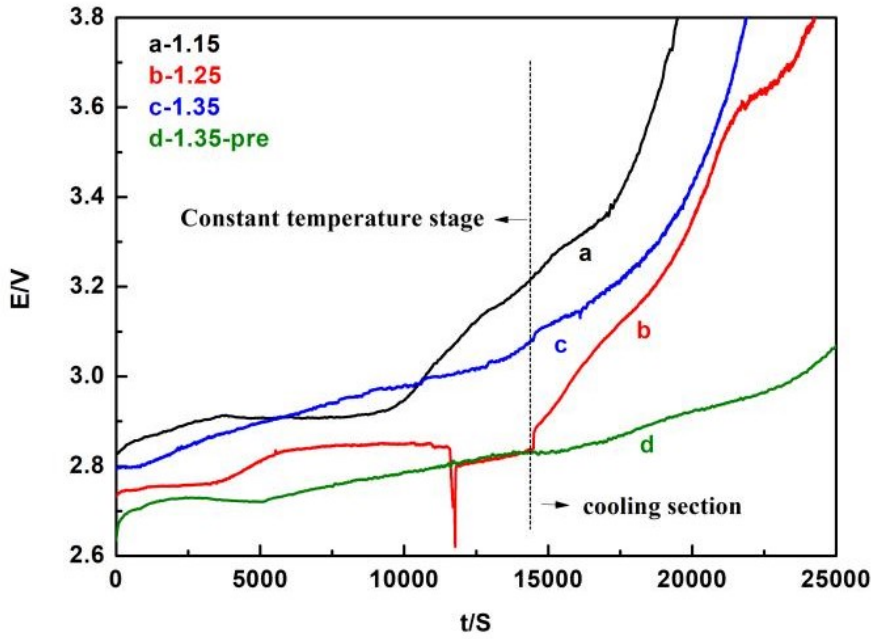

Figure 5. Constant current electrolysis curves of alloy inert anode:
a. bath ratio of 1.15, unpremelted electrolyte before test
b. bath ratio of 1.25, unpremelted electrolyte before test
c. bath ratio of 1.35, unpremelted electrolyte before test
d. bath ratio of 1.35, pre-melted electrolyte for 40 min before test.

Figures 6–9 illustrate the changes in the working voltage of the alloy anode by temperature changes during constant current (0.5 A/cm^2) electrolysis in each electrolyte system. During the cooling process, the working electrode potential exhibited more pronounced fluctuations and a faster rate of potential rise in low molar ratio electrolyte systems (1.15 and 1.25). At 1.15, the voltage rapidly surged to 4 V. At 1.25, the anodic voltage increase accelerated when temperature dropped below 1038 K, with a sharp potential spike occurring at 998 K. For the 1.35 system and non-premelted electrolyte, the anodic potential rise accelerated at 1038 K. In pre-melting electrolyte, rapid voltage increase initiated at 1018 K. Hence, the electrolysis temperature may potentially be maintained above 1038 K for stable tests.

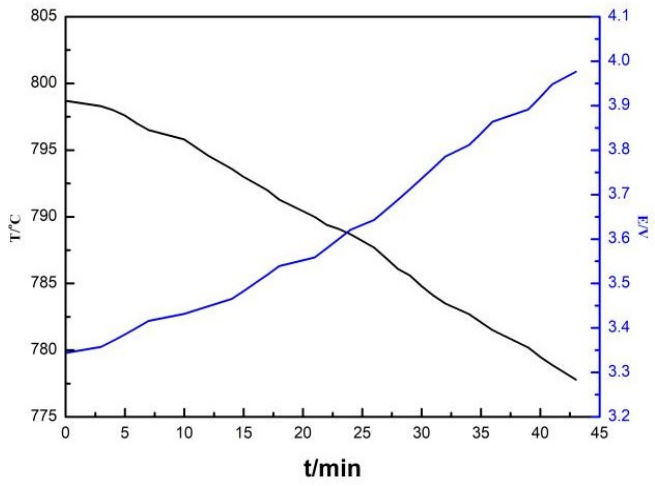

Figure 6. T-E curve of the alloy inert anode for the cooling process in the unpremelted electrolyte of bath ratio of 1.15.

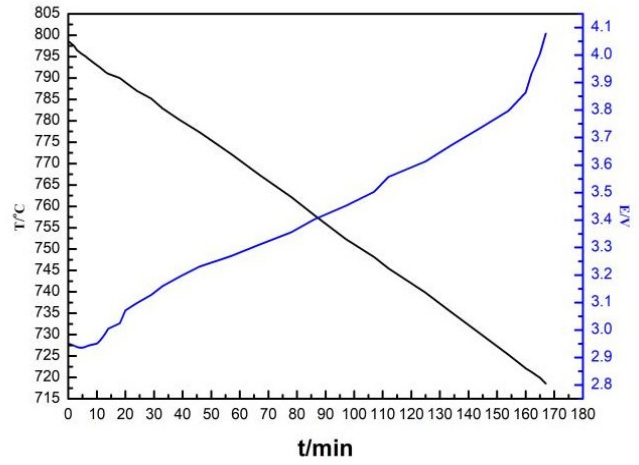

Figure 7. T-E curve of the alloy inert anode of cooling process in the unpremelted electrolyte of bath ratio of 1.25.

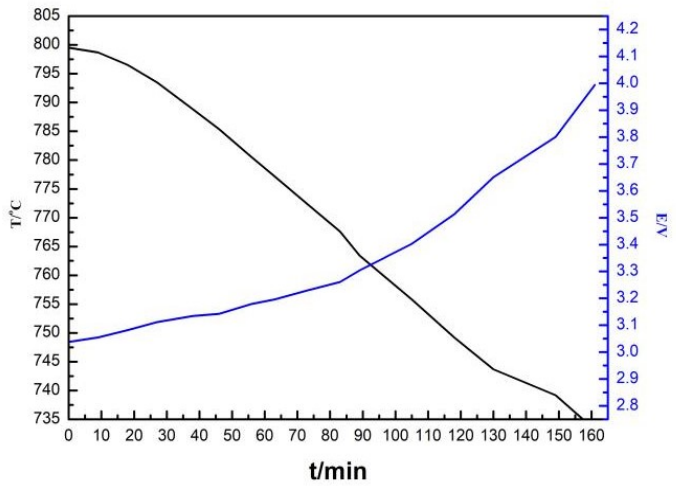

Figure 8. T-E curve of the alloy inert anode of cooling process in the unpremelted electrolyte of bath ratio of 1.35.

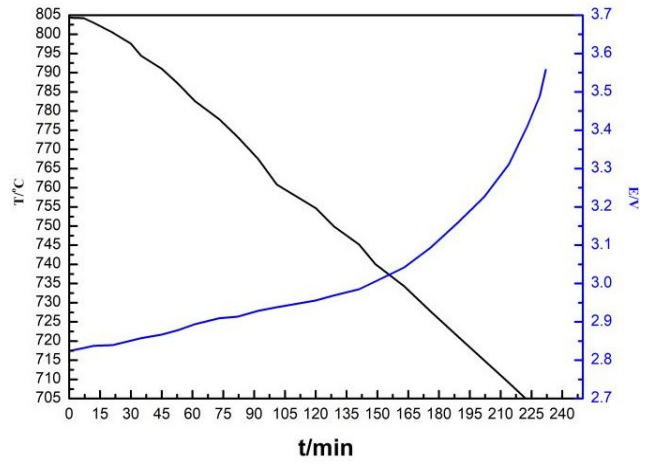

Figure 9. T-E curve of the alloy inert anode of cooling process in the pre-melted electrolyte of bath ratio of 1.35.

3.3 SEM-EDS

After electrolysis at 1073 K in pre-melted aluminium electrolyte with a bath ratio of 1.35, the copper-iron aluminium-based alloy inert anode was cleaned off the surface electrolyte and the cross section was subjected to SEM-EDS analysis. The results of the analyses are shown in Figure 10 and Table 1. From the analysis results, it can be concluded that the oxide film layer of the anode of this alloy is relatively dense, and the outermost layer of the surface is relatively rich in Fe and contains a small amount of F, Na and K. The Cu content is mainly concentrated in the inner part of the oxide film layer near the substrate. Therefore, it is assumed that the migration capacity of Fe ions in the anode during electrolysis is greater than that of Cu ions, and Fe constantly diffuses outward and corrodes preferentially, forming the oxide film layer of Fe covering the most superficial layer of the anode. The closer to the substrate, the richer is the oxide of Cu, which further blocks the erosion of the electrolyte and slows down the corrosion of the anode in the aluminium electrolyte in the near step.

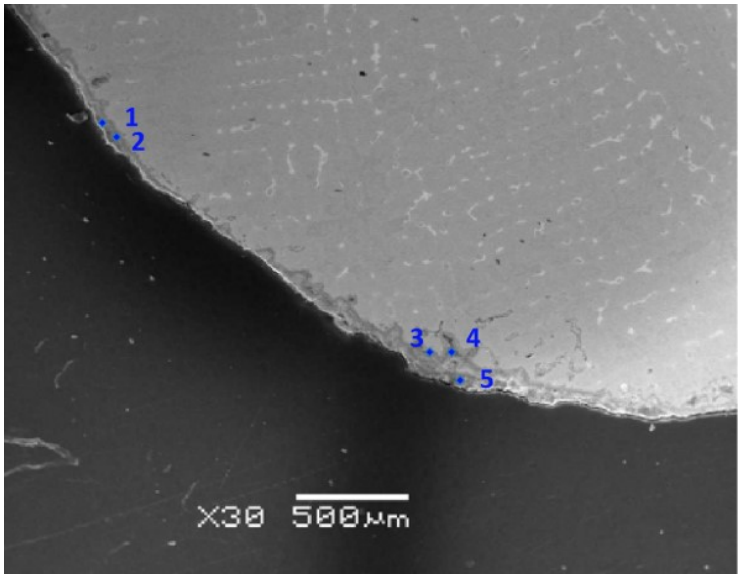

Figure 10. Cross-sectional morphology of the anode after constant current electrolysis at 1073 K.

Table 1. Quantitative results of EDS in anode surface layer after constant current electrolysis at 1073 K (%).

Fig. 10 ref. point	Fe	Cu	O	F	Na	Al	K
1	75.75	0.81	7.10	9.09	3.23	--	4.02
2	70.86	9.89	9.36	7.43	1.11	--	1.35
3	21.14	64.99	5.59	8.28	--	--	--
4	18.39	71.57	6.30	3.57	--	0.2	--
5	73.61	6.16	8.96	6.13	2.02	--	3.12

3.4 Corrosion Rate Analysis

After electrolysis of the copper-iron aluminium-based alloy inert anode in pre-melted aluminium electrolyte with bath ratio of 1.35 at 1073 K at constant current (0.5 A/cm^{-2}), the electrolyte was removed and analysed for impurity content using PE optima 8000 inductively coupled plasma emission spectrometer.

Table 2. Impurity content in the electrolyte after constant current electrolysis at 1073 K (%).

Element	Fe	Cu
content	0.0197	0.0092

The electrode corrosion rate (WR) calculation formula is shown in Equation 1:

$$WR = \frac{m_e \omega_e + m_{Al} \omega_{Al}}{100 \times \rho \times A \times t} \quad (1)$$

where:

WR	Corrosion rate, g/h
m_e	Mass of electrolyte, g
m_{Al}	Mass of primary aluminium produced by electrolysis, g
ω_e	Impurity content in the electrolyte, wt %
ω_{Al}	Impurity content in the primary aluminium, wt %
ρ	Density of anode, g/cm^3
A	Effective working area of anode, cm^2
t	Electrolysis time, h

Aluminium was not found in the electrodes after the tests. This is probably because the effective electrolytic area of the electrode was small and the electrolyte content was limited, and the mass of primary aluminium and its impurity content were negligible in the estimation of the electrode corrosion rate. The addition of aluminium in the alloy inert anode composition for the test is only about 5 %, which is negligible compared with the aluminium content in the electrolyte. The mass of electrolyte for the test was 280 g. The working electrode for the test is cylindrical with an effective electrolytic area of 1.858 cm^2. And the density of the electrode for the test is 8.1 g/cm^3. The annual corrosion rate of the alloy anode is estimated to be about 9.8 mm according to Table 2 and Equation 1. This is too high and we need to further allocate the anode and the electrolyte compositions to reduce the corrosion rate to an acceptable level.

4. Conclusions

From the work presented in this paper, we can draw the following conclusions:

a. At 1073 K, in the electrolyte of the NaF-KF-AlF_3-Al_2O_3 system, with the increase of bath ratio, the concentration or activity of conductive ions in the molten salt increases, and the ions are more easily moved, which is manifested as an increase in current on the linear scanning curve. Alloy inert anode in the higher bath ratio of the low temperature aluminium electrolyte, its self-corrosion resistance is lower, and there is a strong tendency for self-corrosion reaction to occur.
b. The Fe ion migration ability on the surface of the copper-iron aluminium-based alloy anode is larger than that of Cu ions in the electrolysis process. And Fe constantly diffuses outward and corrodes preferentially, forming an oxide film layer of Fe covering the most superficial layer of the anode. The closer it is to the substrate, the richer the oxides of Cu are, which further blocks the erosion of the electrolyte and slows down the proximity corrosion of the anode in the aluminium electrolyte.
c. The oxide film of copper-iron aluminium-based alloy anode combined with oxygen in molten salt electrolyte with relatively high bath ratio will be denser, moderate thickness and relatively stable.
d. When the electrolysis temperature is lower than 1038 K, the anode voltage increases rapidly. The electrolysis temperature of Cu-Fe-Al-based alloy anode in low-temperature aluminium electrolyte is preferably above 1038 K.

e. Low-temperature pre-melting of the electrolyte prior to electrolysis trials effectively will remove or significantly reduce adsorbed water, thereby inhibiting the hydrolysis reaction between aluminum fluoride (AlF_3) and adsorbed water. This suppression minimizes anode corrosion during electrolysis and may lower the electrode potential of the anode. Additionally, electrolyte pre-melting enhances compositional homogeneity. Combined with the electrochemical reaction intensity of alloy anodes and energy efficiency considerations, pre-melted electrolyte potentially extends anode service life and stabilizes long-term electrolysis processes.

5. References

1. Meng Xiu, Jianhua Liu, Progress in the study of corrosion processes of aluminium electrolytic inert anodes in molten electrolyte, *China Nonferrous Metallurgy*, 2024(1), 34-36.
2. Kechao Zhou, Yong He, Zhiyou Li, Ting Shen, Lei Zhang, Aluminium electrolysis inert anode material technology research progress, *Transactions of Nonferrous Metals Society of China*, 2021(11), 3010-3023.
3. Yury A Morozov, Vladimir S Yalunin, Inert anode technology in the concept of green aluminum metallurgy, *RUDN Journal of Engineering Research*, 2022 (23), 15-22.
4. Biao Wang, Feng Liang, Yongnian Dai, Zhiming Yan, Current research status and future development forecast of aluminium electrolysis inert anodes, *Light Metals* 2018(12), 30-34. (Chinese)
5. Wei Wei, Shujiang Geng, Fuhui Wang, Evaluation of Ni-Fe base alloys as inert anode for low-temperature aluminium electrolysis, *Journal of Materials Sciences and Technology*, SCI 2022(107), 216-226.
6. ZhongLiang Tian, YanQing Lai, Jie Li, YeXiang Liu, Effect of Cu-Ni content on the corrosion resistance of (Cu-Ni)/(10NiO-90$NiFe_2O_4$) cermet inert anode for aluminum electrolysis, *Acta Metallurgica Sinica*, 2008(21), 72-78.
7. Jomar Thonstad, Adolf Kisza, Jan Hives, Anode overvoltage on metallic inert anode in low-melting bath, *Light Metals* 2006, 373-377.
8. Haiming Xiao, Rune Hovland, Sverre Rolseth, Jomar Thonstad, Studies on the corrosion and the behavior of inert anodes in aluminum electrolysis, Metallurgical and Materials Transactions B 1996 (27), 185-193.
9. Mark Glucina, Margaret Hyland, Cu-Al Alloy as an anode for aluminium electrowinning, *Corrosion Science*, 2006 (48), 2457-2463.
10. Reidar Haugsud, On the influence of non-protective CuO on high-temperature oxidation of Cu-rich Cu-Ni based alloys, *Oxidation of Metals* 1999, 53 (5-6), 427-431.
11. Jianhong Yang, John N. Hryn, Greg K. Krumdick, Aluminium electrolysis tests with inert anodes in KF-AlF_3-based electrolytes, *Light Metals* 2006, 421-424.
12. Andrey P. Khramov et al., Anodic behaviour of the $Cu_{82}Al_8Ni_5Fe_5$ alloy in low-temperature aluminium electrolysis, *Coros. Sci*. 2013(7), 194-202.